Robust Tracking of the Heating Value in Underground Coal Gasification Process Using Dynamic Integral Sliding Mode Control and a Gain-Scheduled Modified Utkin Observer

Ali Arshad Uppal[a,*], Saif Siddique Butt[b], Qudrat Khan[c], Harald Aschemann[d]

[a]*Department of Electrical Engineering, COMSATS University Islamabad, Pakistan*
[b]*IAV Development GmbH, Gifhorn, Germany*
[c]*Center for Advanced Studies in Telecommunication, COMSATS University Islamabad, Pakistan*
[d]*Chair of Mechatronics, University of Rostock, Rostock, Germany*

Abstract

In this paper, a model-based control and state reconstruction of an underground coal gasification (UCG) process is elaborated. In order to deploy model-based control and estimation strategies, a sophisticated model of the UCG process based on partial differential equations is approximated with a nonlinear control-oriented model that adequately preserves the fundamental dynamic characteristics of the process. A robust dynamic integral sliding mode control (DISMC) is designed for the approximated model to track the desired heating value, which is one of the key indicators for evaluating the performance of an UCG process. In most of the industrial applications, a desired heating value has to be attained. The unknown states required for the model-based control are reconstructed using a gain-scheduled modified Utkin observer (GSMUO). In order to assess the robustness of the nonlinear control and estimation techniques, the water influx phenomenon is considered as an input disturbance. Moreover, the underlying UCG plant model is subjected to parametric variations as well as measurement noise. In order to guarantee the stability of the overall system, the boundedness of the internal dynamics is also proved. To make a fair comparison, the per-

*Corresponding author
Email address: ali_arshad@comsats.edu.pk (Ali Arshad Uppal)

formance of the proposed controller is compared with an integral sliding mode control (ISMC) and a classical PI controller. Simulation results highlight the effectiveness of the proposed control scheme in terms of minimum control energy and improved tracking error.

Keywords: Underground coal gasification control, energy conversion systems, dynamic integral sliding mode control, gain scheduled modified Utkin observer.

---

1. INTRODUCTION

The detrimental impact of coal combustion on both air and water quality has been addressed by the advent of clean coal technologies, which allow the removal of harmful gases before, during and after the burning of coal [1, 2, 3]. Coal has become the leading fuel for electricity production after the introduction of integrated gasification combined cycle (IGCC) technology. In IGCC, coal gasification is integrated with a combined cycle turbine. Gasification is the partial oxidation of coal, which produces synthetic gas or syngas (a mixture of CO, H_2, CH_4 and higher hydrocarbons) that preserves its combustion heat to a maximum extent. The high operating pressure of the gasification process makes the separation of harmful contaminants from useful combustible gases easier, where the latter ones act as fuel for the highly efficient combined cycle turbines to generate electric power [4, 5]. Gasification can either be performed in specially designed chambers – denoted as surface gasification – or the coal seams can be gasified deep under ground – known as underground coal gasification (UCG). In UCG, the ignition of the coal seam is followed by the injection of oxidants through the inlet well, drilled from the surface to the coal seam. The oxidants chemically react with coal to produce syngas, which is withdrawn from the outlet well.

Industrial applications like IGCC require a desired heating value of the syngas [7]. Therefore, one of the key parameters for determining the efficiency of a UCG process is the heating value of syngas. It has been already established in [8] that both composition and flow rate of the injected oxidants can be varied

independently to control the heating value of syngas.

In the literature, both model-free and model-based control techniques have been exploited for the UCG process. In [9] and [10], a conventional PI controller is designed for a lab scale UCG setup to control the concentrations and the temperatures of product gases as well as the heating value. Recently in [11], an optimum controller is designed for maximizing the concentration of CO for the similar UCG setup. The model-based control of UCG for maintaining a desired constant heating value of syngas has been investigated in [12, 13, 14]. In [12], an equivalent control based sliding mode control (SMC) [15] is designed for an approximate model using ordinary differential equations that is based on the assumptions proposed in [16, 17]. Therein, all the state variables are considered to be measurable, which is usually not the case. The super-twisting sliding mode control as well as a conventional sliding mode control design proposed in [13] and [14], respectively, are also based on the approximate models derived from [8]. Moreover, state measurements are not required for the control implementation in both cases. The bounds on the control gains are determined with the approximate models. However, this could lead to a conservative control action, because the upper bounds of the approximate model are employed. The control techniques are then assessed using the sophisticated UCG model [8]. In [18], the mathematical model of [12] is employed to design an integral sliding model control (ISMC) for tracking the heating value of syngas. For the proposed model-based control design, a gain-scheduled modified Utkin observer (GSMUO) [19, 20] is employed to reconstruct the unknown states. Moreover, it has been analytically demonstrated that the zero dynamics of the process under control is stable.

One of the drawbacks of SMC is the chattering phenomenon due to the inclusion of a discontinuous sgn function directly in the control input. In order to account for this limitation, a dynamic integral sliding mode control (DISMC) is proposed in this paper. The DISMC includes the discontinuous sgn function in the time-derivative of the control input, which is needed to be filtered before employing to the plant. Consequently, a continuous control input is obtained

and the chattering phenomenon is reduced significantly, cf. [21]. The controller aims at tracking of desired heating value for the control-oriented model of UCG plant [12] subject to the impact of parametric uncertainties, measurement noise and external disturbances. Furthermore, unknown states of the system are estimated using a GSMUO. Water influx from surrounding aquifers intrudes in the UCG reactor, and converts into steam due to the very high temperature. Hence, the flow-rate of the steam is considered as an input disturbance.

This paper is arranged as follows: In Section 2, the nonlinear control-oriented model of the UCG plant is presented. The DISMC and the GSMUO for the UCG plant are designed in Sections 3 and 4, respectively. The simulation results of the proposed scheme are discussed in Section 5 and the paper is concluded in Section 6.

2. Mathematical Model of UCG Process

In this work, the nonlinear control-oriented model of the UCG process, see [12], is employed for the model-based control design. The model covers eight gases (CO, CO_2, H_2, CH_4, H_2O, O_2, N_2, Tar) and two solids (coal and char). The following ordinary differential equations describe the energy and

mass balances of solids and gases:

$$
\begin{aligned}
\dot{\rho}_{\text{coal}} &= -M_1 R_1 \ , \\
\dot{\rho}_{\text{char}} &= M_2(p_{R_1\text{char}} R_1 - R_2 - R_3), \\
\dot{T}_s &= \frac{1}{C_s}\big(h_t(T - T_s) - \Delta q_2 R_2 - \Delta q_3 R_3\big) \ , \\
\dot{C}_{\text{CO}} &= p_{R_1\text{CO}} R_1 + R_3 - \beta C_{\text{CO}} \ , \\
\dot{C}_{\text{CO}_2} &= p_{R_1\text{CO}_2} R_1 + R_2 - \beta C_{\text{CO}_2} \ , \\
\dot{C}_{\text{H}_2} &= p_{R_1\text{H}_2} R_1 + R_3 - \beta C_{\text{H}_2} \ , \\
\dot{C}_{\text{CH}_4} &= p_{R_1\text{CH}_4} R_1 - \beta C_{\text{CH}_4} \ , \\
\dot{C}_{\text{Tar}} &= p_{R_1\text{Tar}} R_1 - \beta C_{\text{Tar}} \ , \\
\dot{C}_{\text{H}_2\text{O}} &= p_{R_1\text{H}_2\text{O}} R_1 + p_{R_2\text{H}_2\text{O}} R_2 - p_{R_3\text{H}_2\text{O}} R_3 - \beta C_{\text{H}_2\text{O}} + \frac{\Pi}{L} u + \frac{1}{L}\delta \ , \\
\dot{C}_{\text{O}_2} &= -p_{R_2\text{O}_2} R_2 - \beta C_{\text{O}_2} + \frac{\Xi}{L} u \ , \\
\dot{C}_{\text{N}_2} &= -\beta C_{\text{N}_2} + \frac{\Psi}{L} u \ .
\end{aligned} \tag{1}
$$

Although a large number of chemical reactions take place in a UCG reactor, the chemical kinetics of the current model are governed by only three dominant reactions [8], which are stated in Table. 1. The compounds – $CH_{0.912}O_{0.194}$,

Table 1: Dominant chemical reactions in UCG.

Sr.	**Chemical equations**
1.	**Coal pyrolysis**
	$CH_{0.912}O_{0.194} \xrightarrow{R_1} p_{R_1\text{char}} CH_{0.15}O_{0.02} + p_{R_1\text{CO}} CO + p_{R_1\text{H}_2\text{O}} H_2O + p_{R_1\text{H}_2} H_2 + p_{R_1\text{CH}_4} CH_4 + p_{R_1\text{CO}_2} CO_2 + p_{R_1\text{Tar}} (CH_{2.782})_9$
2.	**Char oxidation**
	$CH_{0.15}O_{0.02} + p_{R_2\text{O}_2} O_2 \xrightarrow{R_2} CO_2 + p_{R_2\text{H}_2\text{O}} H_2O$
3.	**Steam gasification**
	$CH_{0.15}O_{0.02} + p_{R_3\text{H}_2\text{O}} H_2O \xrightarrow{R_3} CO + H_2$

$CH_{0.15}O_{0.02}$ and $(CH_{2.782})_9$ – represent molecular formulas of coal, char and

tar, respectively. The corresponding rates of the chemical reactions – R_1, R_2 and R_3 – are expressed as

$$
\begin{aligned}
R_1 &= 5\frac{\rho_{\text{coal}}}{M_1}\exp\left(\frac{-6039}{T_s}\right), R_{m_2} = \frac{1}{10}h_t m_{\text{O}_2}, \\
R_{c_2} &= \frac{1}{M_2}\left(9.55\times 10^8 \rho_{\text{char}} m_{\text{O}_2} P \exp\left(\frac{-22142}{T_s}\right) T_s^{-0.5}\right), \\
R_2 &= \frac{1}{\dfrac{1}{R_{c_2}} + \dfrac{1}{R_{m_2}}}, \; R_{m_3} = \frac{1}{10}h_t m_{\text{H}_2\text{O}}, \\
R_{c_3} &= \frac{\rho_{char} m_{\text{H}_2\text{O}}^2 P^2 \exp\left(5.052 - \dfrac{12908}{T_s}\right)}{M_2\left(m_{\text{H}_2\text{O}} P + \exp\left(-22.216 + \dfrac{24880}{T_s}\right)\right)^2}, \\
R_3 &= \frac{1}{\dfrac{1}{R_{c_3}} + \dfrac{1}{R_{m_3}}},
\end{aligned}
\tag{2}
$$

where m_{O_2} and $m_{\text{H}_2\text{O}}$ are the internal molar fractions of O_2 and H_2O. Mathematically, the molar fractions are given by

$$
\begin{aligned}
m_{\text{O}_2} &= \frac{C_{\text{O}_2}}{C_T + C_{\text{H}_2\text{O}}}, \; m_{\text{H}_2\text{O}} = \frac{C_{\text{H}_2\text{O}}}{C_T + C_{\text{H}_2\text{O}}}, \\
C_T &= C_{\text{CO}} + C_{\text{CO}_2} + C_{\text{H}_2} + C_{\text{CH}_4} + C_{\text{Tar}} + C_{\text{O}_2} + C_{\text{N}_2}.
\end{aligned}
$$

Table 2 lists all the variables along with their meaning that appear in the mathematical model of the UCG process.

The stoichiometric coefficients and the nominal parameter values are listed in Table 3 and Table 4, respectively.

The nonlinear control-oriented model given in (1) can be rewritten in a control-affine form, i.e.,

$$
\dot{\boldsymbol{x}} = \boldsymbol{f}(\boldsymbol{x}) + \boldsymbol{g_1} u + \boldsymbol{g_2}\delta, \tag{3}
$$

where $\boldsymbol{x} \in \mathbb{R}^{11}$ is the state vector, $\boldsymbol{f}, \boldsymbol{g_1}, \boldsymbol{g_2} \in \mathbb{R}^{11}$ are smooth vector fields, u is the control input and δ is the external disturbance, which satisfies the following assumption:

Assumption 1. *Let δ be a matched disturbance and sufficiently smooth, i.e., $\dot{\delta}$*

Table 2: List of parameters and states.

Symbol	**Description**
ρ_i	Density of solid i (g/cm^3)
C_i	Concentration of gas i (mol/cm^3)
M_i	Molecular weight (g/mol), $i = 1, 2$ for coal and char, respectively
T_s, T	Solid and gas temperatures (K)
h_t	Heat transfer coefficient (cal/s/K/cm^3)
C_s	Specific heat capacity of solids (cal/g/K)
R_i	Rate of a chemical reaction (mol/cm^3/s), $i = 1, 2, 3$ represents pyrolysis, char oxidation and steam gasification, respectively
Δq_i	Heat of reaction i (cal/mol), $i = 1, 2$ represents char oxidation and steam gasification, respectively
L	Length of the reactor (cm)
βC_i	Approximation of spatial derivative (mol/cm^3/s)
u	Flow rate of injected gases (moles/cm^2/s)
δ	Input disturbance: flow rate of steam (moles/cm^2/s)
Π, Ξ,Ψ	Percentages of H_2O, O_2 and N_2 in u
P	Gas pressure (atm)
p_{R_ij}	$i \in \{1, 2, 3\}$, j $\in$ {char, CO, CO_2, H_2, CH_4, H_2O, O_2, Tar}

Table 3: Stoichiometric coefficients.

$p_{R_1\text{char}}$	$p_{R_1\text{CO}}$	$p_{R_1\text{CO}_2}$	$p_{R_1\text{H}_2}$	$p_{R_1\text{CH}_4}$	$p_{R_1\text{Tar}}$	$p_{R_1\text{H}_2\text{O}}$	$p_{R_2\text{H}_2\text{O}}$	$p_{R_3\text{H}_2\text{O}}$	$p_{R_2\text{O}_2}$
0.766	0.008	0.058	0.083	0.044	0.0138	0.055	0.075	0.925	1.02

is also continuous and bounded

$$||\dot{\delta}(t)|| \leq \varpi(t) \leq \varpi_0 \ ,$$

where ϖ is a smooth function and $\varpi_0 \in \mathbb{R}^+$.

Table 4: Nominal parameter values.

C_s	β	P	h_t	L	Δq_1	Δq_2
7.3920	7×10^{-6}	4.83	0.001	100	-93929	31309.7

The state vector for the control-oriented model is given by

$$\begin{aligned} \boldsymbol{x} = [\rho_{\text{coal}} \quad \rho_{\text{char}} \quad T_s \quad C_{\text{CO}} \quad C_{\text{CO}_2} \quad C_{\text{H}_2} \\ C_{\text{CH}_4} \quad C_{\text{Tar}} \quad C_{H_2O} \quad C_{\text{O}_2} \quad C_{\text{N}_2}]^T \ . \end{aligned} \tag{4}$$

The product gases recovered from the production well are sent to the gas analyzer through a network of pipes. After removal of steam from the gas mixture, the gas analyzer measures the percent volume content of each dry gas [8, 13]. Therefore, the concentration of the gases can be determined from the known volume content of each gas. Accordingly, the measurement vector $\boldsymbol{y_m}$ is given by

$$\boldsymbol{y_m} = \begin{bmatrix} C_{\text{CO}} & C_{\text{CO}_2} & C_{\text{H}_2} & C_{\text{CH}_4} & C_{\text{Tar}} & C_{\text{O}_2} & C_{\text{N}_2} \end{bmatrix}^T \ . \tag{5}$$

For the given control problem, the heating value H_v of syngas is considered as the controlled variable, which is expressed as

$$H_v = H_{\text{CO}}\chi_{\text{CO}} + H_{\text{H}_2}\chi_{\text{H}_2} + H_{\text{CH}_4}\chi_{\text{CH}_4} \ , \tag{6}$$

where $H_i, i \in \{CO, H_2, CH_4\}$ is the combustion heat (KJ/mol) of gas i and χ_i represents the molar fraction of the gases, characterized by the ratio

$$\chi_i = \frac{C_i}{C_{_T}} \ .$$

The control design aims at maintaining the heating value at predefined set-points depending on the operating conditions, i.e., consumption of coal and char within the UCG bed. Therefore, the subsequent section discusses the design of a dynamic integral sliding model control (DISMC) for the UCG process.

3. Dynamic Integral Sliding Mode Control Design

In this section, a DISMC is designed that tracks the desired trajectory of the heating value H_v of the syngas. DISMC combines the benefits of ISMC and

dynamic SMC and, moreover, yields additional advantages like the elimination of reaching phase with increased robustness and a continuous control input, see [22, 23].

DISMC offers two dynamic terms in its control law, i.e.,

$$\dot{u} = \dot{u}_c + \dot{u}_d \ . \tag{7}$$

The continuous part $\dot{u}_c$ forces the convergence of the states of the nominal system to the desired equilibria – directly after the establishment of SM at t_0 (i.e., when the controller starts its operation). The discontinuous part $\dot{u}_d$ enforces a sliding mode despite modeling uncertainties and external disturbances – also from the very beginning of the controller operation, see [22, 23].

In this paper, $\dot{u}_c$ is designed by using the pole placement technique, which guarantees asymptotic convergence of the tracking error

$$\dot{u}_c = \ddot{e} = -\eta\dot{e} - \zeta e \ , \quad \text{and} \quad e = H_v - H_{v_d} \ , \tag{8}$$

where $\eta, \zeta \in \mathbb{R}^+$ are positive controller gains, and H_{v_d} is the desired heating value. The closed-loop poles are the roots of the polynomial $\rho^2 + \eta\rho + \zeta$, where ρ is a complex variable.

In order to attain a desired robustness and performance, the following integral sliding surface is designed

$$s(e) = \sigma(e) + z \ , \quad \text{and} \quad \sigma(e) = \dot{e} + \lambda e \ , \tag{9}$$

where $\lambda \in \mathbb{R}^+$ is a design variable and z is an integral term chosen as follows

$$\dot{z} = -\lambda\dot{e} - \dot{u}_c \quad \text{with} \quad z(0) = -\sigma(e(0)) \ . \tag{10}$$

The specific choice of the sliding surface and the initial condition of the integral term enforces a sliding mode from the very beginning that eliminates the reaching phase. Therefore, the robustness of the closed-loop system increases right from the beginning.

3.1. Stability of the Nominal System

To prove the stability of the nominal system – in the absence of any uncertainties and the disturbance δ –, the time derivative of (9) is considered along with (7), (8) and (10). This leads to

$$\begin{aligned} \dot{s} &= \ddot{e} - \dot{u}, \\ &= \Omega(\boldsymbol{x}, u, t) - \Upsilon \dot{u}_d - (1 + \Upsilon)\, \dot{u}_c \ . \end{aligned} \tag{11}$$

Herein, $\Upsilon = \frac{\Phi+\Psi}{L} \in \mathbb{R}^+$ and $\Omega(\boldsymbol{x}, u, t)$ are smooth functions of the system states $\boldsymbol{x}$ and the control input u, which are derived from the UCG model (1).

To ensure finite-time enforcement of SM, the reaching condition with a discontinuous controller gain $\kappa \in \mathbb{R}^+$ is selected as follows

$$\dot{s} = -\kappa \operatorname{sgn}(s) \ . \tag{12}$$

Now the discontinuous part of the control input $\dot{u}_d$ is obtained from (11) and (12)

$$\dot{u}_d = -\frac{1}{\Upsilon}\Big(-\Omega(\boldsymbol{x}, u, t) + (\Upsilon + 1)\, \dot{u}_c - \kappa \operatorname{sgn}(s)\Big) \ . \tag{13}$$

Consequently, the control input is obtained by integrating (7). As the discontinuous $\operatorname{sgn}(s)$ appears in the time-derivative of the control input, the control input is continuous, and chattering is reduced significantly [24].

To prove the existence of sliding mode in finite-time, the following Lyapunov function along with its time-derivative are introduced

$$V(\boldsymbol{x}, t) = \frac{1}{2} s^2 \ , \tag{14}$$

$$\dot{V}(\boldsymbol{x}, t) = s\dot{s} \ . \tag{15}$$

The sliding surface s converges to zero if the following condition is fulfilled

$$s\dot{s} < 0 \ . \tag{16}$$

By substituting (13) in (11) and using $s\,\mathrm{sgn}(s) = |s|$, it can be easily shown that the nominal system satisfies (16). The reaching condition is given by

$$s\dot{s} = -\kappa|s| < 0 \ . \tag{17}$$

The result in (17) confirms finite-time convergence, i.e., the sliding surface $s = 0$ is attained in finite time.

3.2. Stability of the Perturbed System

Nevertheless, the original system has a matched input disturbance (water influx δ, cf. (3)) and parametric uncertainties. Therefore, the perturbed $\dot{s}$ is

$$\dot{\tilde{s}} = \Omega(\boldsymbol{x}, u, t) - \Upsilon\dot{u}_d - (\Upsilon + 1)\,\dot{u}_c + g_2\dot{\delta}(t) + \tilde{f}(\boldsymbol{x}, t) \ , \tag{18}$$

where $\dot{\delta}$ and $||\tilde{f}|| \leq \tilde{f}_0$ represent the time-derivative of the external disturbance and modeling uncertainties, respectively.

Substituting (13) in (18) and multiplying with s yields

$$\begin{aligned} s\dot{\tilde{s}} &= s\left(-\kappa\,\mathrm{sgn}(s) + g_2\dot{\delta}(t) + \tilde{f}(\boldsymbol{x}, t)\right), \\ &= -\kappa|s| + sg_2\dot{\delta}(t) + s\tilde{f}(\boldsymbol{x}, t), \\ &\leq -\kappa|s| + |s|\varpi_0||g_2|| + |s|\tilde{f}_0, \\ &\leq -|s|\left(\kappa - \varpi_0||g_2|| - \tilde{f}_0\right) \ . \end{aligned} \tag{19}$$

If $\kappa \geq \xi + \varpi_0||g_2|| + \tilde{f}_0$ holds, with $\xi \in \mathbb{R}^+$, then the time derivative becomes

$$\dot{V} \leq -\sqrt{2V}\xi \ . \tag{20}$$

The inequality in (20) shows that the system trajectories reach the sliding manifold in finite-time t_s [19], given by

$$t_s \leq \frac{\sqrt{2V(s(0))}}{\xi} \ . \tag{21}$$

The dynamics of the system under sliding motion is governed by

$$s = 0 \wedge \dot{s} = \ddot{e} + \eta\dot{e} + \zeta e = 0 \ . \tag{22}$$

Since η and ζ are positive constants, the tracking error asymptotically converges to zero according to the Hurwitz's stability criterion.

3.3. Stability of the Zero Dynamics

After the establishment of a sliding mode at $t = t_0$, it is mandatory to check the stability and boundedness of the zero dynamics. When the tracking error converges to zero, i.e., $H_v = H_{v_d}$ holds, the following equation can be derived

$$H_{CO}C_{CO} + H_{H_2}C_{H_2} + H_{CH_4}C_{CH_4} = C_T H_{v_d} \ . \tag{23}$$

This equation gives a unique solution for only one C_i. Therefore, the boundedness of the zero dynamics has to be determined. Using (23), the boundedness of C_{CO} follows from

$$C_{CO} = \frac{\left(\tilde{C}_T H_{v_d} - H_{H_2}C_{H_2} - H_{CH_4}C_{CH_4}\right)}{H_{CO} - H_{v_d}} \ , \tag{24}$$

where $\tilde{C}_T$ is the sum of concentrations of all the gases except CO.

During sliding mode, $\dot{u} = \dot{u}_d$ holds, because $\dot{u}_c$ in (8) becomes zero. Moreover, by substituting $\mathrm{sgn}(\sigma) = 0$ and $\Omega(\boldsymbol{x}, u, t) = -Ku_d + \Gamma(\boldsymbol{x}, u_d, t)$ in (13), $\dot{u}_d$ reduces to

$$\dot{u}_d = \frac{1}{\Upsilon}\left(-Ku_d + \Gamma\right) \ , \tag{25}$$

where K is a strictly positive constant.

The zero dynamics of the UCG process involves all state equations of (1) – except the dynamics of $\dot{C}_{CO}$. As a result, the zero dynamics can be written in the following form

$$\begin{aligned} \dot{\boldsymbol{x}}(t) &= \Lambda \boldsymbol{x}(t) + \omega(\boldsymbol{x}, u_d, t) \ , \\ \Lambda &= diag\left(-\varepsilon; -\varrho; -\frac{h_t}{C_s}; -\beta; -\beta; -\beta; -\beta; -\beta; -\beta; -\beta\right), \end{aligned} \tag{26}$$

where $\boldsymbol{x} \in \mathbb{R}^{10}$, $\omega(\boldsymbol{x}, u_d, t) \in \mathbb{R}^{10}$ is the nonlinear function of $\boldsymbol{x}$ and u_d, $\Lambda \in \mathbb{R}^{10\times 10}$ is a constant matrix and $\varepsilon, \varrho \in \mathbb{R}^+$ are given by

$$\varepsilon = \exp\left(\frac{-6039}{T_{s_{max}}}\right) \quad and \quad \varrho = M_2\left(\tilde{R}_2 + \tilde{R}_3\right)\Big|_{T_{s_{max}}} \ , \tag{27}$$

with $T_{s_{max}} = \max_{t>t_0} T_s$ and $R_i = \rho_{\mathrm{char}}\tilde{R}_i$.

Prior to the evaluation of the boundedness of the zero dynamics, it is worth mentioning that mass and energy balances of solids and gases in (1) are coupled with each other by the reaction rates (2). These are highly nonlinear functions of the system states, especially T_s, because all the reaction rates require a certain temperature level to occur [8]. Now, if $0 < T_{s_{max}} \leq \infty$ holds, $\varepsilon \to 0$ according to (27), then ρ_{char} in (1) and R_1 in (2) asymptotically converge to zero. As in UCG coal is decomposed into char and product gases by R_1, according to the law of conservation of energy $\max_t \rho_{\text{char}} < \rho_{\text{coal}}(0)$ holds, which implies that ρ_{char} is also bounded. With bounded ρ_{coal} and ρ_{char} as well as $0 < T_{s_{max}} \leq \infty$, all the reaction rates are also bounded, cf. (2). By using the energy balance in (1) and the fact that the reaction rates are bounded, $T_s \leq T_{s_{max}} < \infty$ holds according to the input $T_g \leq T_{g_{max}}$. Moreover, due to the physical properties of the system, both $\boldsymbol{x}(t)$ and u are positive.

In the light of above results, $0 < \Gamma \leq \nu(t)$ and $0 < \omega \leq \mu(t)$ in (25) and (26), respectively, are also bounded, because they are functions of the reaction rates. Therefore, the maximum value of the control input $\bar{u}_d(t)$ can be obtained by solving the linear differential equation in (25) by substituting $\Gamma = \nu(t)$

$$\bar{u}_d(t) = u_d(t_0) \exp\Big(- \frac{K}{\Upsilon} t\Big) + \int_{t_0}^{t} \exp\Big(- \frac{K}{\Upsilon} (t - \tau)\Big) \nu(\tau) d\tau \ . \tag{28}$$

As $\nu(t)$ is bounded, therefore, $\bar{u}_d(t)$ is also bounded $\forall t \geq t_0$. By substituting $\omega = \mu(t)$, see [25], the solution of (26) yields the maximum value of the state vector $\bar{\boldsymbol{x}}(t)$

$$\bar{\boldsymbol{x}}(t) = \boldsymbol{x}(t_0) \exp\Big(\Lambda\,(t - t_0)\Big) + \int_{t_0}^{t} \exp\Big(\Lambda\,(t - \tau)\Big) \mu(\tau) d\tau \ . \tag{29}$$

The matrix Λ is Hurwitz and $\mu(t)$ is bounded, hence, the zero dynamics of the system is also bounded $\forall t \geq t_0$. Consequently, using the results of (28) and (29) in (24), it can be shown that C_{CO} is bounded as well.

The function $\Omega(\boldsymbol{x}, u, t)$ in (13) depends on the state vector $\boldsymbol{x}(t)$, which is not completely measurable. Therefore, a gain-scheduled modified Utkin observer (GSMUO) is designed to reconstruct the unknown states of the system.

4. Gain-Scheduled Modified Utkin Observer

The GSMUO is based on a quasi-linear model of the UCG, which is obtained by the linearization of (1). In case of a non-zero equilibrium and arbitrary operating points, the linearization approach based on a first-order Taylor series expansion fails to provide an appropriate linear dynamics of a nonlinear model [26]. To overcome this issue, a constrained minimization problem is formulated with the goal to construct a linear model in $\boldsymbol{x}$, u and δ that approximates the behavior of (3) in the vicinity of the operating point $\boldsymbol{x}_{op}$. For any u and δ, the exact decomposition of the control-affine system (3) yields

$$\dot{\boldsymbol{x}} = \boldsymbol{f}(\boldsymbol{x}) + \boldsymbol{g_1}u + \boldsymbol{g_2}\delta = \boldsymbol{A}(\boldsymbol{x})\boldsymbol{x} + \boldsymbol{g_1}u + \boldsymbol{g_2}\delta \ . \tag{30}$$

Likewise, the control-affine system at the operating point $\boldsymbol{x}_{op}$ can be given as follows

$$\dot{\boldsymbol{x}}_{op} = \boldsymbol{f}(\boldsymbol{x}_{op}) + \boldsymbol{g_1}u + \boldsymbol{g_2}\delta = \boldsymbol{A}(\boldsymbol{x}_{op})\boldsymbol{x}_{op} + \boldsymbol{g_1}u + \boldsymbol{g_2}\delta \ . \tag{31}$$

The problem is to find a state-dependent matrix $\boldsymbol{A(x)}$ such that in a neighborhood of $\boldsymbol{x}_{op}$

$$\boldsymbol{f}(\boldsymbol{x}) = \boldsymbol{A}(\boldsymbol{x})\boldsymbol{x} \ , \text{ and } \boldsymbol{f}(\boldsymbol{x}_{op}) = \boldsymbol{A}(\boldsymbol{x}_{op})\boldsymbol{x}_{op} \ . \tag{32}$$

Let $\boldsymbol{a}_i^T$ denote the ith row of the matrix $\boldsymbol{A}$. Then, (32) can be re-written as

$$f_i(\boldsymbol{x}) = \boldsymbol{a}_i^T(\boldsymbol{x})\boldsymbol{x} \ , \quad i = 1, 2, \ldots, n \ , \tag{33}$$

and

$$f_i(\boldsymbol{x}_{op}) = \boldsymbol{a}_i^T(\boldsymbol{x}_{op})\boldsymbol{x}_{op} \ . \tag{34}$$

Expanding the left-hand side of (33) around $\boldsymbol{x}_{op}$, and neglecting the higher-order terms leads to

$$f_i(\boldsymbol{x}) = f_i(\boldsymbol{x}_{op}) + \nabla^T f_i(\boldsymbol{x}_{op})(\boldsymbol{x} - \boldsymbol{x}_{op}) = \boldsymbol{a}_i^T(\boldsymbol{x})\boldsymbol{x} \ , \tag{35}$$

where $\nabla^T f_i(\boldsymbol{x}) \in \mathbb{R}^{n\times 1}$ is the gradient of f_i evaluated at $\boldsymbol{x}$. Using (34), the above equation can be rewritten as

$$\nabla^T f_i(\boldsymbol{x}_{op})(\boldsymbol{x}-\boldsymbol{x}_{op}) = \boldsymbol{a}_i^T(\boldsymbol{x}_{op})(\boldsymbol{x}-\boldsymbol{x}_{op}) \ . \tag{36}$$

In order to find $\boldsymbol{a}_i$, a constrained minimization problem is formulated as

$$\begin{aligned} \underset{\boldsymbol{a}_i}{\text{minimize}} \quad & J = \frac{1}{2}||\nabla f_i(\boldsymbol{x}_{op}) - \boldsymbol{a}_i(\boldsymbol{x}_{op})||_2^2 \\ \text{subject to} \quad & f_i(\boldsymbol{x}_{op}) = \boldsymbol{a}_i^T(\boldsymbol{x}_{op})\boldsymbol{x}_{op} \ . \end{aligned}$$

The first-order optimality condition for the augmented cost function $\bar{J}$

$$\bar{J} = \frac{1}{2}||\nabla f_i(\boldsymbol{x}_{op}) - \boldsymbol{a}_i(\boldsymbol{x}_{op})||_2^2 + \lambda(f_i(\boldsymbol{x}_{op}) - \boldsymbol{a}_i^T(\boldsymbol{x}_{op})\boldsymbol{x}_{op}) \ , \tag{37}$$

with λ as a Lagrange multiplier, results in $\nabla_{\boldsymbol{a}_i}\bar{J} = 0$, i.e.,

$$\boldsymbol{a}_i = \nabla f_i(\boldsymbol{x}_{op}) - \lambda \boldsymbol{x}_{op} \ . \tag{38}$$

The Lagrange multiplier λ is determined by pre-multiplying (38) with $\boldsymbol{x}_{op}^T$ and substituting in (34). Provided that $\boldsymbol{x}_{op} \neq \boldsymbol{0}$ holds, this results in

$$\lambda = \frac{\boldsymbol{x}_{op}^T \nabla f_i(\boldsymbol{x}_{op}) - f_i(\boldsymbol{x}_{op})}{||\boldsymbol{x}_{op}||^2} \ . \tag{39}$$

Substituting (39) into (38) leads to

$$\boldsymbol{a}_i = \nabla f_i(\boldsymbol{x}_{op}) + \frac{f_i(\boldsymbol{x}_{op}) - \boldsymbol{x}_{op}^T \nabla f_i(\boldsymbol{x}_{op})}{||\boldsymbol{x}_{op}||^2}\boldsymbol{x}_{op} \ , \quad \boldsymbol{x}_{op} \neq \boldsymbol{0} \ . \tag{40}$$

It is worth mentioning that if the operating point is an equilibrium point, i.e., $\boldsymbol{x}_{op} = \boldsymbol{0}$, the above formulation reduces to the first-order linear approximation of a nonlinear system, where the system matrix becomes the Jacobian of the nonlinear vector on the right-hand side.

Using the formulation above, the nonlinear control-oriented model of the UCG can be stated as a quasi-linear model, i.e.,

$$\begin{aligned} \dot{\boldsymbol{x}} &= \boldsymbol{A}(\boldsymbol{x})\boldsymbol{x} + \boldsymbol{b}u \ , \\ \boldsymbol{y} &= \boldsymbol{C}\boldsymbol{x} \ , \end{aligned} \tag{41}$$

where $\boldsymbol{x} \in \mathbb{R}^{11}$, $\boldsymbol{A}(\boldsymbol{x}) \in \mathbb{R}^{11\times 11}$, $\boldsymbol{b} \in \mathbb{R}^{11}$ and $\boldsymbol{C} \in \mathbb{R}^{7\times 11}$. The matrices $\boldsymbol{b}$ and $\boldsymbol{C}$ can be directly written from (1) and (5).

In a conventional sliding mode observer, it is difficult to choose discontinuous gains to enforce a sliding mode in finite-time. The issue is resolved by incorporating a Luenberger-type gain matrix within the sliding mode observer, which provides a feedback of the output errors to achieve a robust state reconstruction [27]. To design the GSMUO, the system needs to be transformed into a special state space representation with state vector $\tilde{\boldsymbol{x}} = [\boldsymbol{z} \quad \boldsymbol{y}_m]^T = \boldsymbol{T}\boldsymbol{x}$. The transformation matrix is chosen as

$$\boldsymbol{T} = \begin{bmatrix} \boldsymbol{N}^T & \boldsymbol{C} \end{bmatrix}^T, \tag{42}$$

where $\boldsymbol{N}_c \in \mathbb{R}^{4\times 7}$ spans the null space of $\boldsymbol{C}$.

The transformed linear system is given by

$$\begin{bmatrix} \dot{\boldsymbol{z}} \\ \dot{\boldsymbol{y}}_m \end{bmatrix} = \boldsymbol{T}\boldsymbol{A}(\boldsymbol{x})\boldsymbol{T}^{-1} \begin{bmatrix} \boldsymbol{z} \\ \boldsymbol{y}_m \end{bmatrix} + \boldsymbol{T}\boldsymbol{b}u \ . \tag{43}$$

According to new coordinates transformation, the unknown states are

$$\boldsymbol{z} = \begin{bmatrix} \rho_{\text{coal}} & \rho_{\text{char}} & T_s & C_{\text{H}_2\text{O}} \end{bmatrix}^T. \tag{44}$$

The corresponding output matrix is

$$\boldsymbol{C}\boldsymbol{T}^{-1} = \begin{bmatrix} \boldsymbol{0}_{4\times 7} & \boldsymbol{I}_{7\times 7} \end{bmatrix} \ . \tag{45}$$

Now, the new system can be partitioned as follows

$$\boldsymbol{T}\ \boldsymbol{A}(\boldsymbol{x})\ \boldsymbol{T}^{-1} = \left[\begin{array}{c:c} \boldsymbol{A}_{11}(\boldsymbol{x}) & \boldsymbol{A}_{12}(\boldsymbol{x}) \\ \hdashline \boldsymbol{A}_{21}(\boldsymbol{x}) & \boldsymbol{A}_{22}(\boldsymbol{x}) \end{array}\right] \ , \text{ and } \ \boldsymbol{T}\ \boldsymbol{b} = \left[\begin{array}{c} \boldsymbol{b}_1 \\ \hdashline \boldsymbol{b}_2 \end{array}\right] \ .$$

Rewriting the system dynamics leads to

$$\begin{aligned} \dot{\boldsymbol{z}} &= \boldsymbol{A}_{11}(\boldsymbol{x})\boldsymbol{z} + \boldsymbol{A}_{12}(\boldsymbol{x})\boldsymbol{y}_m + \boldsymbol{b}_1 u \ , \\ \dot{\boldsymbol{y}}_m &= \boldsymbol{A}_{21}(\boldsymbol{x})\boldsymbol{z} + \boldsymbol{A}_{22}(\boldsymbol{x})\boldsymbol{y}_m + \boldsymbol{b}_2 u \ . \end{aligned} \tag{46}$$

The overall structure of the corresponding GSMUO is given by

$$\begin{aligned} \dot{\hat{\boldsymbol{z}}} &= \boldsymbol{A}_{11}(\boldsymbol{x})\hat{\boldsymbol{z}} + \boldsymbol{A}_{12}(\boldsymbol{x})\hat{\boldsymbol{y}}_m + \boldsymbol{b}_1 u + \boldsymbol{L}\boldsymbol{v} - \boldsymbol{G}_1\boldsymbol{e}_y \ , \\ \dot{\hat{\boldsymbol{y}}}_m &= \boldsymbol{A}_{21}(\boldsymbol{x})\hat{\boldsymbol{z}} + \boldsymbol{A}_{22}(\boldsymbol{x})\hat{\boldsymbol{y}}_m + \boldsymbol{b}_2 u - \boldsymbol{v} - \boldsymbol{G}_2\boldsymbol{e}_y \ . \end{aligned} \tag{47}$$

Here, $\hat{\boldsymbol{z}}$ and $\hat{\boldsymbol{y}}_m$ are the estimates of unknown and known states, respectively. The gain matrices $\boldsymbol{G}_1 \in \mathbb{R}^{4\times 7}$ and $\boldsymbol{G}_2 \in \mathbb{R}^{7\times 7}$ represent the Luenberger-type gain matrices, which provide robustness against certain class of uncertainties. Furthermore, $\boldsymbol{L} \in \mathbb{R}^{4\times 7}$ is a feedback gain matrix. The vector $\boldsymbol{\upsilon} \in \mathbb{R}^7$ is defined by

$$\boldsymbol{\upsilon} = \begin{bmatrix} M_1 \ \mathrm{sgn}(\hat{y}_{m,1} - y_{m,1}) \\ M_2 \ \mathrm{sgn}(\hat{y}_{m,2} - y_{m,2}) \\ \vdots \\ \vdots \\ M_7 \ \mathrm{sgn}(\hat{y}_{m,7} - y_{m,7}) \end{bmatrix}, \tag{48}$$

with $M_i \in \mathbb{R}^+$. By using (46) and (47), the dynamics of the estimation error can be expressed as

$$\dot{\hat{\boldsymbol{e}}}_z = \boldsymbol{A}_{11}(\boldsymbol{x})\hat{\boldsymbol{e}}_z + \boldsymbol{A}_{12}(\boldsymbol{x})\hat{\boldsymbol{e}}_y + \boldsymbol{L}\boldsymbol{\upsilon} - \boldsymbol{G}_1\boldsymbol{e}_y \ , \tag{49}$$

$$\dot{\hat{\boldsymbol{e}}}_y = \boldsymbol{A}_{21}(\boldsymbol{x})\hat{\boldsymbol{e}}_z + \boldsymbol{A}_{22}(\boldsymbol{x})\hat{\boldsymbol{e}}_y - \boldsymbol{\upsilon} - \boldsymbol{G}_2\boldsymbol{e}_y \ , \tag{50}$$

where $\boldsymbol{e}_z = \hat{\boldsymbol{z}} - \boldsymbol{z}$ and $\boldsymbol{e}_y = \hat{\boldsymbol{y}}_m - \boldsymbol{y}_m$. Introducing a new error variable $\bar{\boldsymbol{e}}_z = \boldsymbol{e}_z + \boldsymbol{L}\,\boldsymbol{e}_y$, the transformed error dynamics with states $\bar{\boldsymbol{e}}_z$ and $\boldsymbol{e}_y$ is given by

$$\left[\begin{array}{c} \dot{\bar{\boldsymbol{e}}}_z \\ \hdashline \dot{\boldsymbol{e}}_y \end{array}\right] = \left[\begin{array}{c:c} \bar{\boldsymbol{A}}_{11} & \bar{\boldsymbol{A}}_{12} \\ \hdashline \boldsymbol{A}_{21}(\boldsymbol{x}) & \bar{\boldsymbol{A}}_{22} \end{array}\right] \left[\begin{array}{c} \bar{\boldsymbol{e}}_z \\ \hdashline \boldsymbol{e}_y \end{array}\right] + \left[\begin{array}{c} \boldsymbol{0} \\ \hdashline -\boldsymbol{I} \end{array}\right] \boldsymbol{\upsilon}\,, \tag{51}$$

with the submatrices

$$\begin{aligned} \bar{\boldsymbol{A}}_{11} &= \boldsymbol{A}_{11}(\boldsymbol{x}) + \boldsymbol{L}\,\boldsymbol{A}_{21}(\boldsymbol{x}) \ , \\ \bar{\boldsymbol{A}}_{12} &= \boldsymbol{A}_{12}(\boldsymbol{x}) - \bar{\boldsymbol{A}}_{11}\boldsymbol{L} - \boldsymbol{G}_1 + \boldsymbol{L}\,(\boldsymbol{A}_{22}(\boldsymbol{x}) - \boldsymbol{G}_2) \ , \\ \bar{\boldsymbol{A}}_{22} &= \boldsymbol{A}_{22}(\boldsymbol{x}) - \boldsymbol{G}_2 - \boldsymbol{A}_{21}(\boldsymbol{x})\,\boldsymbol{L} \ . \end{aligned} \tag{52}$$

According to (51), the state estimation problem has been transformed into a regulation problem in $\boldsymbol{e}_y$ and $\bar{\boldsymbol{e}}_z$, with $\boldsymbol{\upsilon}$ as an auxiliary observer input. The selection of each discontinuous gain M_i in (48) satisfies the reaching condition $e_{y_i}\dot{e}_{y_i} < 0$, where e_{y_i} is the sliding variable. This can be proved by considering

the following Lyapunov function

$$V_i = \frac{1}{2} e_{y_i}^2 \ . \tag{53}$$

The time-derivative of (53) along (51), yields

$$\begin{aligned} \dot{V}_i &= e_{y_i} \left(\boldsymbol{A}_{21_i}(\boldsymbol{x}) \bar{\boldsymbol{e}_z} + \bar{\boldsymbol{A}}_{22_i} e_{y_i} - \upsilon_i \right) \ , \\ &\leq -|e_{y_i}| \left(M_i - |\boldsymbol{A}_{21_{(i)}}(\boldsymbol{x}) \bar{\boldsymbol{e}_z} + \bar{\boldsymbol{A}}_{22_{(i)}} e_{y_i}| \right) \ , \end{aligned} \tag{54}$$

where $\boldsymbol{A}_{21_{(i)}}(\boldsymbol{x})$ and $\bar{\boldsymbol{A}}_{22_{(i)}}$ represent the i^{th} row of matrices $\boldsymbol{A}_{21}(\boldsymbol{x})$ and $\bar{\boldsymbol{A}}_{22}$ respectively. Now if $M_i \geq \varsigma + |\boldsymbol{A}_{21_{(i)}}(\boldsymbol{x}) \bar{\boldsymbol{e}_z} + \bar{\boldsymbol{A}}_{22_{(i)}} e_{y_i}|$, then

$$\dot{V}_i = -\sqrt{2V_i}\varsigma \ ,$$

and the measurement error converges to zero in finite-time [19], i.e., $e_{y_i} \to 0$ given by

$$t_s \leq \frac{\sqrt{2V_i(0)}}{\varsigma} \ .$$

Moreover, if $\boldsymbol{L}$ is designed in such a way that the matrix $\bar{\boldsymbol{A}}_{11}^*$ according to

$$\boldsymbol{A}_{11}(\boldsymbol{x}) + \boldsymbol{L}\, \boldsymbol{A}_{21}(\boldsymbol{x}) = \bar{\boldsymbol{A}}_{11}^* \tag{55}$$

is Hurwitz, then the error $\boldsymbol{e}_z$ converges asymptotically as well. Similarly, $\boldsymbol{G}_2$ can be chosen to render the design matrix $\bar{\boldsymbol{A}}_{22}^*$ Hurwitz, with

$$\boldsymbol{A}_{22}(\boldsymbol{x}) - \boldsymbol{G}_2 - \boldsymbol{A}_{21}(\boldsymbol{x})\, \boldsymbol{L} = \bar{\boldsymbol{A}}_{22}^* \ . \tag{56}$$

The gain matrices $\boldsymbol{L}$ and $\boldsymbol{G}_2$ are computed using the LQR method, which minimizes a quadratic cost functional and leads to eigenvalues of $\bar{\boldsymbol{A}}_{11}^*$ and $\bar{\boldsymbol{A}}_{22}^*$ in $\mathbb{C}^-$ in the left half complex plane. Finally, $\boldsymbol{G}_1$ in (52) can be designed in such a way that the equality $\bar{\boldsymbol{A}}_{12}(\boldsymbol{x}) = \boldsymbol{0}$ holds. An appropriate choice of $\boldsymbol{L}$, $\boldsymbol{G}_2$ and $\boldsymbol{G}_1$ will result in the asymptotic convergence of the error dynamics, i.e., $\boldsymbol{e}_z \to 0$ as $t \to \infty$. Hence a proper state observation is confirmed.

5. Results and Discussions

In this section, simulation results of UCG process along with the DISMC and GSMUO are presented. Moreover, a comparison is also carried out between the designed DISMC, ISMC [18] and a classical PI controller for trajectory tracking regarding the desired heating value. In order to mimic the real time scenario, a rigorous simulation analysis is performed by considering the following practical issues:

- The composition of the inlet gas mixture is $O_2 = 15.4\%$, $H_2O = 77\%$ and $N_2 = 7.6\%$, based on the composition $\Pi = 0.77$, $\Xi = 0.154$ and $\Psi = 7.6$ in (1).
- An additive white Guassian noise with zero mean and variance of 4×10^{-4} is added in each measured C_i of the UCG plant. This variance corresponds to the typical measurement accuracy of the gas analyzer used in the UCG process [8, 13].
- In order to study the robustness property of the control and estimation strategies, parametric uncertainties of 2% are introduced in the nominal system parameters, namely P, β, h_t and C_s in the UCG plant, cf. Table. 5. It is worth mentioning that both the DISMC and the GSMUO use the nominal system parameters.

Table 5: Parameters subjected to perturbations.

Symbol	**Nominal Value**	**Actual Value**
C_s	7.3920	7.244
β	7×10^{-6}	6.86×10^{-6}
P	4.83	4.93
h_t	0.001	0.00102

- The desired trajectory for the heating value is shown in Fig. 1. Ideally a controller should keep H_v at its maximum value. However, in parallel

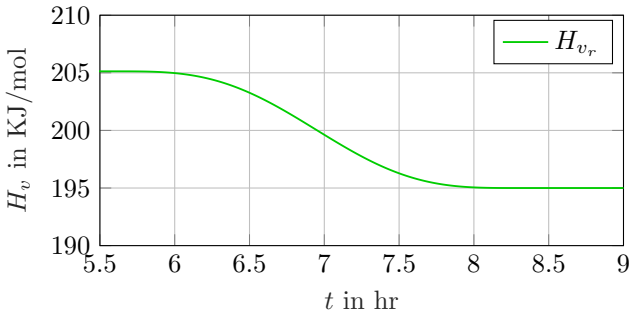

Figure 1: Desired heating value trajectory of syngas during open and closed-loop operations.

to the consumption of coal and char within the UCG bed, the peak value of H_v is decreasing. By ensuring positive flow rates – in order to get a maximum available H_v – a corresponding trajectory is designed for the desired H_v.

- It is important to mention that the UCG process is operated in open-loop for 20000 s to guarantee that the heating value reaches a desired set-point. For this purpose, the flow rate of the injected gases is kept at 2×10^{-4} moles/cm^2/s till 20000 s. Afterwards, the UCG plant is operated in a closed control loop.

- The GSMUO is active during both the open-loop and closed-loop operations of UCG plant.

- Apart from parametric uncertainties, a matched input disturbance δ is also considered to evaluate the robustness of the closed-loop system. The flow rate δ of the steam generated by water influx from surrounding aquifers represents the input disturbance. The time profile for δ is shown in Fig. 2. It is worth pointing out that the steam influx is introduced as soon as the system is under closed-loop control.

In order to study the estimation behavior of the observer, it is necessary to initialize both the UCG plant and GSMUO with different initial conditions. The initial states vectors for the nonlinear control-oriented model of the UCG process

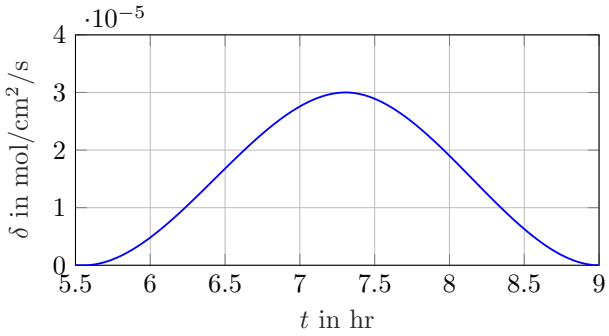

Figure 2: Flow rate of water influx from surrounding aquifers.

and the GSMUO are chosen $\boldsymbol{x}(0) = [0.5\ 0\ 497\ 0\ 0\ 0\ 0\ 0\ 0\ 4.2e{-}4\ 1.6e{-}3]^T$, and $\hat{\boldsymbol{x}}(0) = [0.48\ 0\ 480\ 0\ 0\ 0\ 0\ 0\ 0\ 4.2e{-}4\ 1.6e{-}3]^T$, respectively. Due to the chemical nature of the process, the initial concentration of the gases are known beforehand, hence, initialized with the identical numerical values.

As mentioned in Section 4, the observer gain matrices $\boldsymbol{L}$ and $\boldsymbol{G}_2$ in (55) and (56) are designed using a LQR formulation. This, on the one hand, allows for specifying relative weights to the unknown states and measurements. On the other hand, an optimal gain can be obtained for the given operating conditions of the quasi-linear model of the UCG plant. For gain matrix $\boldsymbol{L}$, the weighting matrices $\boldsymbol{Q}$ and $\boldsymbol{R}$ representing the weights for $\boldsymbol{e_z}$ and $\boldsymbol{e_y}$ in the LQR cost function are chosen as

$$\begin{aligned} \boldsymbol{Q} &= \mathrm{diag}(\Theta_1^2; \Theta_2^2; \Theta_3^2; \Theta_4^2)\ , \ \text{and} \\ \boldsymbol{R} &= \mathrm{diag}(\Phi_1^2; \Phi_2^2; \Phi_3^2; \Phi_4^2; \Phi_5^2; \Phi_6^2; \Phi_7^2)\ . \end{aligned} \tag{57}$$

where $\Theta_i, i \in \{1, \ldots, 4\}$ and $\Phi_j, j \in \{1, \ldots, 7\}$ are given by

$$\Theta_i = \zeta\left(\frac{\theta_i}{\boldsymbol{z}_{i\,max}^2}\right)\ , \ \text{and} \ \ \Phi_j = \left(\frac{\phi_j}{\boldsymbol{e}_{y,j\,max}^2}\right)\ .$$

The values of the constants θ_i and ϕ_j are chosen in such a way that the state reconstruction and the measurement error convergence are sufficiently fast. The value ζ characterizes the relative weight between $\boldsymbol{Q}$ and $\boldsymbol{R}$. In case of $\boldsymbol{G}_2$, both $\boldsymbol{Q} \in \mathbb{R}^{7\times 7}$ and $\boldsymbol{R} \in \mathbb{R}^{7\times 7}$ are chosen to facilitate rapid convergence of $\boldsymbol{e_y}$.

Furthermore, the discontinuous gain M_i in (48) needs to satisfy the inequality

$$M_i > ||(\boldsymbol{A}_{21}(x))_i \bar{\boldsymbol{e}}_z + (\bar{\boldsymbol{A}}_{22}(x))_i + \boldsymbol{e}_y||_\infty \ , \tag{58}$$

where i represents the i_{th} row of a matrix. The following discontinuous gains are selected for the observer in (47)

$$M = 10^{-7} \begin{bmatrix} 10 & 18 & 10 & 8 & 22 & 22 & 3 \end{bmatrix}^T .$$

The closed-loop operation starts at 20000 s (5.5 hrs), when H_v reaches its maximum value. Fig. 3 shows the trajectory tracking of H_v for the DISMC, ISMC and PI controllers. To compare the performance of different controllers, the integral gain is kept the same for the DISMC, ISMC and PI controllers. Moreover, the discontinuous gains for DISMC and ISMC, and proportional gain for PI are also identical.

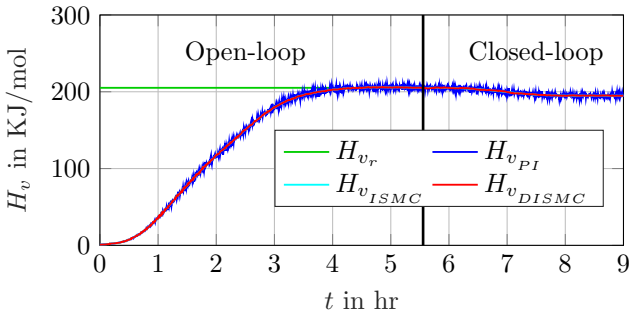

Figure 3: Heating value of the syngas during open-loop and closed-loop operation.

The corresponding tracking error is shown in Fig. 4. The tracking error is shown from that time onwards when the controller is brought into operation.

The control effort for the controllers is depicted in Fig. 5. It can be clearly seen that DISMC consumes minimum control effort to achieve the desired control objective in the presence of parametric uncertainty and input disturbance. Moreover – unlike PI and ISMC – the injected flow rate does not saturate for DISMC. In order to quantitatively evaluate the performance of the controllers,

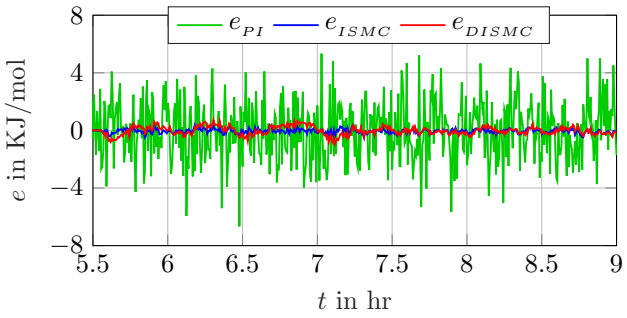

Figure 4: Tracking error for different controllers during closed-loop operation.

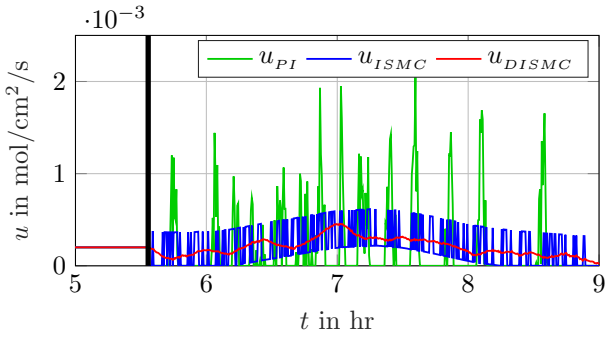

Figure 5: Control input for different controllers.

the root-mean-square error (RMSE) given by

$$\text{RMSE} = \sqrt{\frac{1}{N}\sum_{i=1}^{N} e(i)^2} \ , \quad e(i) = H_v(i) - H_{v_r}(i) \ , \tag{59}$$

is computed, where N is the number of samples. Furthermore, the RMSE value is calculated from the point in time, when the plant is switched to closed-loop operation. Another performance criterion relates to the control effort for each controller. The average power of the control signal for different controllers is computed according to

$$\text{P}_{\text{avg}} = \frac{1}{N}\sum_{i=1}^{N} u(i)^2 \ . \tag{60}$$

The RMSE and the control effort for the controllers are given in Table. 6.

Here, it can be seen that the PI controller leads to a poor performance in

Table 6: RMSE and P_{avg} for different controllers.

Controller	**RMSE**	$\mathbf{P}_{\text{avg}}$
PI	2.1524	6.6607×10^{-7}
ISMC	0.1599	1.1650×10^{-7}
DISMC	0.2880	5.0698×10^{-8}

terms of both tracking error and average power consumption – as compared to the model-based control schemes. Although the RMSE value for the ISMC is smaller than the one for the DISMC, this comes at the cost of a high control action. Fig. 6 shows the time profile of the sliding variable for DISMC given by (9). One of the major advantages of ISMC is the elimination of the reaching

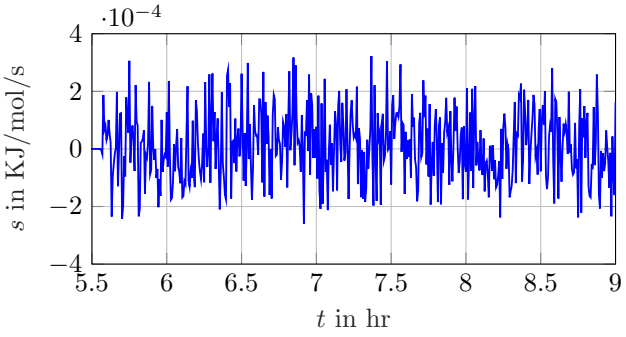

Figure 6: Sliding manifold for DISMC.

phase, which increases the robustness of SMC. It can be seen in Fig. 6 that the sliding mode ($s = 0$) has been established at the very beginning of the controller operation – thereby eliminating the reaching phase. It is evident from the results in Figs. 5 and 6 that DISMC provides a smooth control input and the reaching phase is also eliminated by selecting appropriate initial condition for the integral part of sliding variable, cf. (10). Therefore, DISMC is a hybrid technique, which inherits the advantages of both ISMC and dynamic SMC.

An optimum amount of steam H_2O (g) is required for a successful UCG operation. Too much steam H_2O (g), however, may decrease the temperature of the reactor, and in the extreme case the UCG process can even be extinguished.

It is worth mentioning that a suitable reactor temperature is required for various chemical reactions to occur. On the other hand, a reduced amount of steam H_2O (g) can result in the decrease of gasification reactions, hence the production of syngas can be affected. It can be seen from Fig. 2 and Fig. 5, when water influx δ starts increasing, that the controller injects more oxidants in the cavity to increase the concentration of O_2. Consequently, the temperature of the cavity favors the desired production of syngas. When δ starts decreasing, the moles of the inlet gases are reduced as well to limit the char oxidation reaction, which favors the production of CO_2, which in turn causes a decrease in the amount of syngas. In short, the controller efficiently accounts for the water influx problem.

The subsequent simulation results demonstrate the performance of GSMUO. The concentrations of measured and estimated gases are shown in Fig. 7 and Fig. 8.

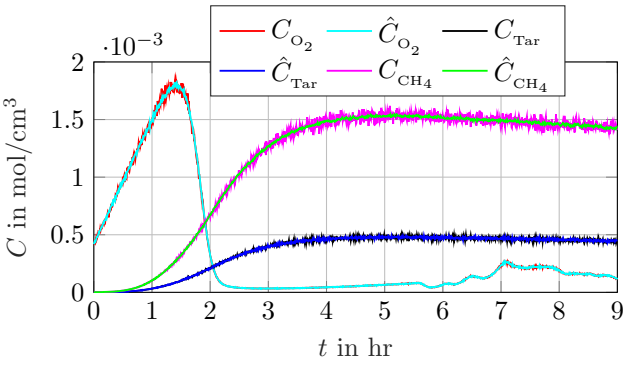

Figure 7: Actual and estimated concentrations of gases.

Herein, the GSMUO also filters out the measurement noise introduced in the UCG plant. It is important to mention that O_2, H_2O (g) and N_2 are the injected gases. O_2 is responsible for char oxidation reaction, which facilitates the pyrolysis and gasification reactions by setting a desired temperature of the reactor. However, H_2O (g) is a fundamental reactant in gasification reactions. The product gases – CO, CO_2, H_2, CH_4 and tar – are generated as a result of the chemical reactions given in Table. 1.

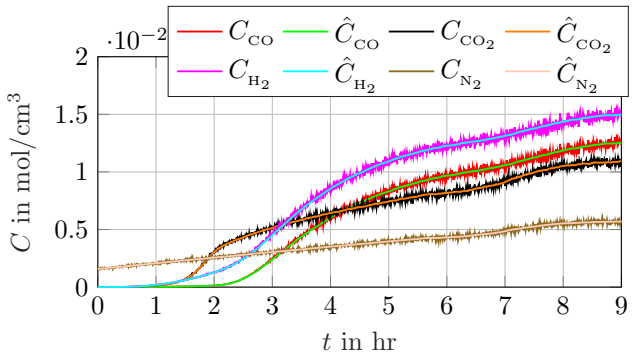

Figure 8: Actual and estimated concentrations of gases.

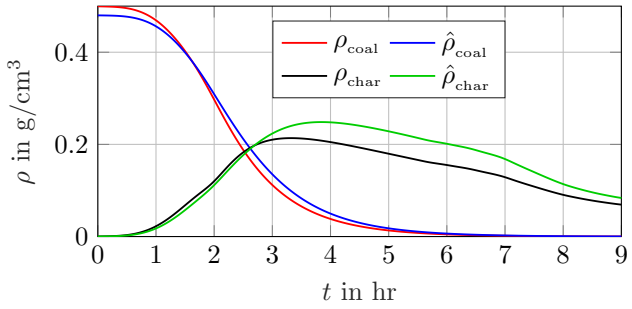

Figure 9: Actual and reconstructed solid densities.

The reconstruction of the unknown states of the UCG model is depicted in Fig. 9, Fig. 10 and Fig. 11. It can be seen from the results that the estimated and true states are in good agreement.

The reconstructed reaction rates based on the estimated states are shown in Fig. 12. When the controller starts operation, almost all the coal is consumed by the reactant gases (see Fig. 9). Therefore, the reaction zone is dominated by char oxidation and steam gasification reactions. The limiting reactants for char oxidation and steam gasification reactions are O_2 and H_2O (g), respectively. Therefore, the char oxidation reaction follows the trend of the O_2 concentration, cf. Fig 7, and the magnitude of the steam gasification reaction is proportional to the water influx δ. In short, the controller manipulates the flow rate of the injected gases to obtain a desired profile for the chemical reactions, which in

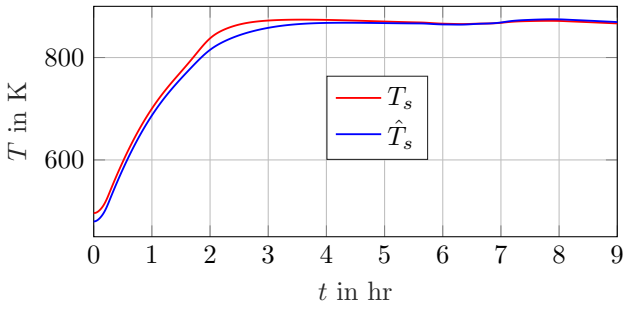

Figure 10: Actual and reconstructed solid temperature.

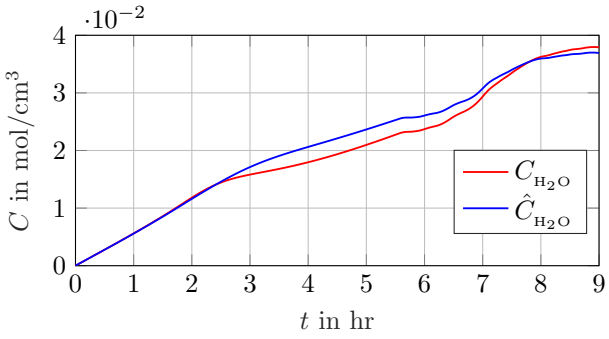

Figure 11: Actual and reconstructed steam concentration.

turn yields the desired H_v.

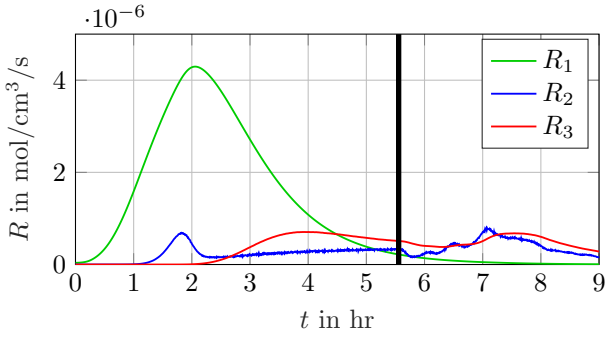

Figure 12: Rates of the chemical reactions considered in the model.

6. Conclusion

In this paper, a model-based DISMC is designed to track the desired heating value for the UCG process. To enable feedback control, the unknown states of the plant are reconstructed using a GSMUO. The design of this estimator is based on a quasi-linear second-order representation of the nonlinear control-oriented model. To make the state reconstruction robust, the gain matrices for the observer are designed using a LQR method and are adapted by gain-scheduling techniques. Moreover, it has been shown that the zero dynamics of the system is bounded. The simulation results demonstrate the effectiveness of the combination of DISMC and GSMUO to achieve the desired control objective in the presence of parametric uncertainties, input disturbance and measurement noise. A quantitative comparison is also made between DISMC, ISMC and PI controllers, which shows that the DISMC performs the desired task with the minimum control effort. This research work serves as a prototype for the development of a model-based control strategy for a field scale UCG process.

References

[1] G. Perkins, Underground coal gasification–Part I: Field demonstrations and process performance, Progress in Energy and Combustion Science 67 (2018) 158 – 187.

[2] G. Perkins, Underground coal gasification–Part II: Fundamental phenomena and modeling, Progress in Energy and Combustion Science 67 (2018) 234 – 274.

[3] A. W. Bhutto, A. A. Bazmi, G. Zahedi, Underground coal gasification: From fundamentals to applications, Progress in Energy and Combustion Science 39 (1) (2013) 189 – 214.

[4] A. Pettinau, F. Ferrara, V. Tola, G. Cau, Techno-economic comparison between different technologies for co2-free power generation from coal, Applied Energy 193 (2017) 426 – 439.

[5] A. Skorek-Osikowska, ukasz Bartela, J. Kotowicz, Thermodynamic and ecological assessment of selected coal-fired power plants integrated with carbon dioxide capture, Applied Energy 200 (2017) 73 – 88.

[6] N. V. Gnanapragasam, B. V. Reddy, M. A. Rosen, Hydrogen production from coal gasification for effective downstream CO_2 capture, International Journal of Hydrogen Energy 35 (10) (2010) 4933 – 4943.

[7] G. M. P. Perkins, Mathematical modelling of underground coal gasification, Ph.D. thesis, The University of New South Wales (2005).

[8] A. A. Uppal, A. I. Bhatti, E. Aamir, R. Samar, S. A. Khan, Control oriented modeling and optimization of one dimensional packed bed model of underground coal gasification, Journal of Process Control 24 (1) (2014) 269–277.

[9] K. Kostúr, J. Kačúr, The monitoring and control of underground coal gasification in laboratory conditions, Acta Montanistica Slovaca 13 (1) (2008) 111–117.

[10] K. Kostur, J. Kacur, Development of control and monitoring system of UCG by promotic, in: 2011 12th International Carpathian Control Conference (ICCC), 2011, pp. 215 –219.

[11] K. Kostur, J. Kacur, Extremum seeking control of carbon monoxide concentration in underground coal gasification, IFAC-PapersOnLine 50 (1) (2017) 13772 – 13777, 20th IFAC World Congress.

[12] A. Arshad, A. Bhatti, R. Samar, Q. Ahmed, E. Aamir, Model development of ucg and calorific value maintenance via sliding mode control, in: 2012 International Conference on Emerging Technologies (ICET), 2012, pp. 1–6.

[13] A. A. Uppal, A. I. Bhatti, E. Aamer, R. Samar, S. A. Khan, Optimization and control of one dimensional packed bed model of underground coal gasification, Journal of Process Control 35 (2015) 11 – 20.

[14] A. A. Uppal, Y. M. Alsmadi, V. I. Utkin, A. I. Bhatti, S. A. Khan, Sliding mode control of underground coal gasification energy conversion process, IEEE Transactions on Control Systems Technology PP (99) (2017) 1–12.

[15] A. Fossard, T. Floquet, An overview of classical sliding mode control, in: J. P. Barbot, W. Perruquetti (Eds.), Sliding Mode Control in Engineering, Control Engineering, Marcel Dekker, Inc., New York, NY, USA, 2002.

[16] A. Winslow, Numerical model of coal gasification in a packed bed, Symposium (International) on Combustion 16 (1) (1977) 503 – 513.

[17] C. B. Thorsness, R. B. Rozsa, Insitu coal-gasification: Model calculations and laboratory experiments, Society of Petroleum Engineers Journal 18 (1978) 105–116.

[18] A. A. Uppal, S. S. Butt, A. I. Bhatti, H. Aschemann, Integral sliding mode control and gain-scheduled modified utkin observer for an underground coal gasification energy conversion process, in: 23rd International Conference on Methods and Models in Automation and Robotics, MMAR, 2018.

[19] C. Edwards, S. Spurgeon, Sliding Mode Control: Theory And Applications, Series in Systems and Control, Taylor & Francis, 1998.

[20] Y. Xiong, M. Saif, Sliding mode observer for nonlinear uncertain systems, IEEE Transactions on Automatic Control 46 (12) (2001) 2012–2017.

[21] J. Liu, X. Wang, Advanced sliding mode control for mechanical systems, design, analysis and matlab simulation (2011).

[22] Q. Khan, A. I. Bhatti, M. Iqbal, Q. Ahmed, Dynamic Integral Sliding Mode Control for SISO Uncertain Systems, International Journal of Innovative Computing, Information and Control 8 (7A) (2012) 4621–4633.

[23] Q. Khan, A. I. Bhatti, S. Iqbal, M. Iqbal, Dynamic integral sliding mode for mimo uncertain nonlinear systems, International Journal of Control, Automation and Systems 9 (1) (2011) 151–160.

[24] H. Sira-Ramirez, On the dynamical sliding mode control of nonlinear systems, International Journal of Control 57 (5) (1993) 1039–1061.

[25] W. L. Brogan, Modern Control Theory (3rd Ed.), Prentice-Hall, Inc., Upper Saddle River, NJ, USA, 1991.

[26] M. C. M. Teixeira, S. H. Zak, Stabilizing controller design for uncertain nonlinear systems using fuzzy models, IEEE Transactions on Fuzzy Systems 7 (2) (1999) 133–142.

[27] S. S. Butt, R. Prabel, H. Aschemann, Second-order sliding mode control of an innovative engine cooling system, in: IECON 2015 - 41st Annual Conference of the IEEE Industrial Electronics Society, 2015, pp. 002479–002484.